Comparison of different sloshing speedmeters

View the article online for updates and enhancements.

Comparison of different sloshing speedmeters

S H Huttner[1,4], S L Danilishin[2,3], S Hild[2,3] and K A Strain[1]

[1] SUPA, School of Physics and Astronomy, University of Glasgow, Glasgow G12 8QQ, United Kingdom
[2] Maastricht University, Faculty of Science and Engineering, PO Box 616, 6200 MD Maastricht, The Netherlands
[3] Nikhef, Science Park 105, 1098 XG Amsterdam, The Netherlands

E-mail: sabina.huttner@glasgow.ac.uk

Abstract

By numerical simulation, we compare the performance of four speedmeter interferometer configurations with potential application in future gravitational wave detectors. In the absence of optical loss, all four configurations can be adjusted to yield the same sensitivity in a fair comparison. Once we introduce a degree of practicality in the form of lossy optics and mode mismatch, however, the situation changes: the sloshing Sagnac and the speedmeter of Purdue and Chen have almost identical performance showing smaller degradation from the ideal than the speedmeter of Freise and the speedmeter of Miao. In a further step, we show that there is a similar hierarchy in the degree of improvement obtained through the application of 10 dB squeezing to the lossy speedmeters. In this case, the sensitivity of each speedmeter improves, but it is greatest for the sloshing Sagnac and the speedmeter of Purdue and Chen, in particular in the lower part of the target frequency range.

Keywords: gravitational wave detector, speedmeter, interferometer

(Some figures may appear in colour only in the online journal)

1. Introduction

The detection of gravitational waves [1] was accomplished using laser-interferometric detectors. In the near future the network of detectors is to be extended [2–6], facilitating sources

---

[4]Author to whom any correspondence should be addressed.

of gravitational waves to be more accurately located in the sky, and extending the range of observational science that may be achieved. In the longer term the community shares a goal of implementing a network of even more sensitive instruments. When considering how to further enhance the sensitivity of gravitational wave detectors, we note that the current detectors are position-sensing detectors, and as such are subject to quantum back-action in the form of radiation-pressure noise which sets a boundary for the low-frequency performance of these conventional instruments. Indeed the current instruments are expected to approach the standard quantum limit (SQL) within the next few years, for mirror masses of order 40 kg. Although techniques such as heavier mirrors and combinations of filter cavities with squeezed light can to some extent suppress this back-action noise, our current work concerns an alternative approach based on velocity-sensing devices, generally called *speedmeters* [7], that can eliminate radiation-pressure noise by design at least in the ideal case. Implementation of speedmeter-based detectors may be an effective route to meeting our aim to enable detection of more, and also more distant sources of gravitational waves.

In general, instruments which offer the possibility of surpassing the SQL are called quantum non-demolition (QND) devices. While several QND methods have been identified, in this paper we restrict ourselves to speedmeters that are able to be implemented using established interferometric techniques. Position metres of the kind employed thus far reach the SQL at a single frequency, or in a narrow band; speedmeters, however, feature quantum-noise limited performance that 'naturally' follows the SQL as a function of frequency over a relatively wide band. Such detectors, therefore, provide a practical approach to obtaining improved performance over a significant band at the lower-end of the gravitational wave spectrum that is accessible to detection on Earth, i.e. broadly from 1 Hz up to around 100 Hz. In this work we therefore focus on methods that yield high sensitivity within this band.

Several speedmeter topologies have been discovered [8–17]. These all work by eliminating position information from the measurement output thereby satisfying the requirements of a QND measurement. This is accomplished by, in effect, cancelling position measurements separated by a short interval of time. To achieve this within a laser-interferometric detector, signal-carrying light is stored for a short period after which it is superposed with signal-containing light from a later time such that position information cancels. The methods we consider are all based on the process of storing the light and feeding it back into the system with the appropriate time delay, or phase shift, and this approach is called sloshing.

In this work we consider two known classes of *sloshing speedmeter*: the *sloshing Michelson speedmeter* and the *sloshing Sagnac speedmeter*. These instruments have the practical advantage of being able to be built from the same functional units as existing position-metre designs, namely combinations of linear optical cavities with additional mirrors and beam-splitters operating with light of a single polarisation. They employ neither ring cavities nor do they require novel application of polarising optics, techniques that are under consideration as alternative approaches to speedmeter design, but which have a range of practical difficulties that currently require investigation.

The Michelson sloshing speedmeter exists in three different variants, and we consider these in historical order: the first is that proposed by Purdue and Chen [10]; the second is that from Miao [18]; and the third was proposed by Freise [19]. The configurations described by Miao and Freise are progressive simplifications of the original Purdue and Chen speedmeter, by leaving one or two mirrors out. More details can be found in section 3. We compare the sensitivity of these Michelson sloshing speedmeters to each other and to that of the sloshing Sagnac speedmeter, proposed by one of us (S D), and previously analysed in [16].

To allow the detection of gravitational-wave induced signal-sidebands, speedmeters, in common with other approaches, require the extremely-weak signal-containing light to be

mixed with a stronger local oscillator light. Here we assume the use of a balanced homodyne signal readout as this method is becoming standard for future detector designs [20]. In the models presented below, a numerical phase shift was employed to adjust the phase of the homodyne field to maximise the signal to noise ratio snr.

In a detector limited predominantly by quantum noise, a common technique to further improve the snr is to apply squeezed light, or more precisely, squeezed vacuum [21]. With the correct and potentially frequency-dependent choice of the squeezing phase, this process can reduce the quantum noise over a significant part of the measurement band. In this respect, speedmeters as a class have an advantage over position metres, as within the range of frequencies in which speedmeter behaviour is exhibited, a single, frequency-independent squeezing phase suffices. In a practical system with optical cavities in the arms of the detector, the storage time of the cavities affects the response near and above the 'corner frequency' represented by the low-pass filtering action of the cavities—typically in the order of 100 Hz in modern gravitational wave detectors. Optimisation of squeezing over the complete frequency band requires frequency-dependent squeezing, even in the case of a speedmeter, and is beyond the scope of the current work. We concentrate instead on the frequency band between the sub-1 Hz mechanical modes of the mirror suspensions and the cavity corner frequency which is around 80 Hz for the specific example system described below. In this context, we explore the performance of the four speedmeters under consideration by including in our models the option of applying 10 dB squeezing, an amount of squeezing that is expected to be entirely practical in the time-frame of the future gravitational wave detectors. For ease of comparing results we choose to optimise the models for performance at a frequency of 10 Hz, broadly in the middle of the band where the systems exhibit a speedmeter response. The exact choice of optimisation frequency within this band is inconsequential in terms of the conclusions that are drawn. Further detail of the optimisation procedure is given below.

In section 2, we introduce the required theory to describe the interferometers in question. Section 3 introduces the four speedmeters in more detail and considers their performance with ideal lossless mirrors. In that section we establish the parameters chosen to ensure a fair comparison that provides closely-similar sensitivity spectra for the four cases. In section 4, we introduce loss into the model, considering its effect on all of the optical components of the speedmeters, and discuss the differences that emerge in their performance. In section 5, we introduce squeezing to our lossy speedmeters, observing that these differences become more pronounced. We present our conclusion in section 6.

2. Quantum noise

The speedmeter introduced by Purdue and Chen is extensively discussed in [9, 10], including details of the effect of losses and the application of squeezing. Similarly, Miao provides a general description, of the system we identify eponymously, in his thesis [18], and Freise described his further-simplification of the approach in his presentation [19]. For the sloshing-Sagnac [16], there exists a description without consideration of loss or squeezing. The derivation, discussion and comparison of the theory, including losses and squeezing for all these speedmeters is beyond the scope of this paper. We present a brief introduction and general outline of how the relevant calculations are performed for the Michelson sloshing speedmeter, noting that these methods underpin the numerical simulations employed to obtain results presented in the subsequent sections. For the interested reader, a more detailed analysis can be found in [9, 10, 22].

The quantum noise of an interferometer is usually described by the two-photon formalism introduced by Caves and Schumaker [23, 24] that represents the input and output light fields at a fixed location in the interferometer in terms of quadrature amplitudes:

$$\hat{E}^{\text{in}}(t) = \mathcal{E}_0 \left[(A^{\text{in}} + \hat{a}_{\text{c}}^{\text{in}}) \cos \omega_{\text{p}} t + \hat{a}_{\text{s}}^{\text{in}} \sin \omega_{\text{p}} t \right], \tag{1}$$

$$\hat{E}^{\text{out}}(t) = \mathcal{E}_0 \left[(B_{\text{c}}^{\text{out}} + \hat{b}_{\text{c}}^{\text{out}}) \cos \omega_{\text{p}} t + (B_{\text{s}}^{\text{out}} + \hat{b}_{\text{s}}^{\text{out}}) \sin \omega_{\text{p}} t \right]. \tag{2}$$

with $\mathcal{E}_0 = \sqrt{4\pi\hbar\omega_{\text{p}}/(\mathcal{A}c)}$ is a normalisation constant defined in the second quantisation of a monochromatic light beam with the carrier frequency ω_{p}, reduced Planck constant $\hbar$ and cross-sectional area $\mathcal{A}$; $A^{\text{in}} = \sqrt{2P^{\text{in}}/(\hbar\omega_{\text{p}})}$ (B^{out}) is the classical mean amplitude of the input (output) light at frequency ω_{p} and optical power P^{in}; $\hat{a}_{\text{c,s}}$ $(\hat{b}_{\text{c,s}})$ describe small, zero-mean quantum fluctuations and variations due to the signal, and they are related to the creation and annihilation operators through

$$\hat{a}_{\text{c}} = \frac{\hat{a} + \hat{a}^{\dagger}}{\sqrt{2}}, \quad \text{and} \quad \hat{a}_{\text{s}} = \frac{\hat{a} - \hat{a}^{\dagger}}{i\sqrt{2}}. \tag{3}$$

Input/output-relations allow us to evaluate the light fields at any location within the optical system, and thereby understand the propagation of quantum noise throughout the interferometer. Analysis of the full interferometer, including losses and imperfections, usually requires to solve a quite extended system of equations, which is normally too large to be tractable analytically (see section 2 of [25]). This task is best suited for numerical simulation software, e.g., FINESSE [26], which is used in this work. Yet to grasp the main features of the quantum noise behaviour, it is sufficient to consider a symmetric, resonance-tuned and loss-free model of the interferometer, which has a particularly simple form of I/O-relations that read:

$$\hat{b}_{\text{c}}^{\text{out}} = e^{2i\beta} \hat{a}_{\text{c}}^{\text{in}}, \tag{4}$$

$$\hat{b}_{\text{s}}^{\text{out}} = e^{2i\beta} \left(\hat{a}_{\text{s}}^{\text{in}} - \mathcal{K}\hat{a}_{\text{c}}^{\text{in}} \right) + e^{i\beta} \sqrt{2\mathcal{K}} \frac{h}{h_{\text{SQL}}}. \tag{5}$$

where h is the sensitivity of the interferometer, that is, the noise of the detector expressed as an equivalent gravitational wave strain spectral density, $h_{\text{SQL}} = \sqrt{8\hbar/(ML^2\Omega^2)}$ is the SQL of the effective differential arm degree of freedom with reduced mass M, Ω is the gravitational wave frequency, L is the arm length, $\mathcal{K}$ is the configuration-specific optomechanical coupling factor of the interferometer introduced by Kimble *et al* [22], β is the additional phase shift light sidebands acquire as they travel in the interferometer, and $\hat{a}_{\text{c,s}}^{\text{in}}$ and $\hat{b}_{\text{c,s}}^{\text{out}}$ stand for the spectra of the cosine and sine quadratures of the sideband fields entering and leaving the signal port of the interferometer. The Fourier transform for the entering fields is:

$$\hat{a}_{\text{c,s}}(t) = \int_{-\infty}^{\infty} \frac{d\Omega}{2\pi} \hat{a}_{\text{c,s}}(\Omega) e^{-i\Omega t}. \tag{6}$$

The explicit equations that define $\mathcal{K}$ for each of the considered speedmeter variants appear to be very close to each other and grasped by the two coupled cavity model, outlined in the original proposal by Braginsky and Khalili [7] and later adopted for optical interferometry in [8]. Apart from different auxiliary optics, the integral part of the studied speedmeters is a 'sloshing' optical cavity placed in the output port of the standard Fabry–Perot–Michelson interferometer. The GW signal 'sloshes' back and forth between the two effective coupled

cavities with an alternating sign and the sloshing rate $\Omega_s = \frac{c}{2}\sqrt{\frac{T_s}{LL_s}}$ defined by the transmittance T_s of the sloshing cavity's *input coupler* and the length of the sloshing cavity L_s.

The corresponding general formula for the Michelson sloshing speedmeter optomechanical coupling factor can be written as follows:

$$\mathcal{K}_{SSM}(\Omega) = \frac{T_s \mathcal{K}_{MI} \sin^2 \alpha_{SC}}{\cos^2(\beta_{MI} + \alpha_{SC}) + T_s R_s \cos^2 \beta_{MI} - T_s \cos(\beta_{MI} + 2\alpha_{SC})} \tag{7}$$

where $\mathcal{K}_{MI}$ and β_{MI} are the optomechanical coupling factor and a frequency-dependent phase shift the modulation sidebands acquire as they pass through the interferometer:

$$\mathcal{K}_{MI} = \frac{\Theta_{MI}\tau}{\Omega^2} \frac{1 - R_{ITM}^2}{1 - 2\sqrt{R_{ITM}} \cos 2\Omega\tau + R_{ITM}} \simeq \frac{2\Theta_{MI}\gamma_{arm}}{\Omega^2(\gamma_{arm}^2 + \Omega^2)}, \tag{8}$$

$$\beta_{MI} = \arctan\left(\frac{1 + \sqrt{R_{ITM}}}{1 - \sqrt{R_{ITM}}} \tan \Omega\tau\right) \simeq \arctan(\Omega/\gamma_{arm}), \tag{9}$$

with $\Theta_{MI} = 4\omega_p P_c/(McL)$ is the normalised intra cavity power, where P_c is the optical power circulating in the interferometer, $T_{ITM} = 1 - R_{ITM}$ is the transmittance of the input test mass of the arm cavities, R_s is the reflectance of the input coupler of the sloshing cavity, τ is the light travel time at distance L, and $\gamma_{arm} = T_{ITM}/(4\tau)$ is the half-bandwidth of the arm cavity. The approximate equality sign indicates the approximation that GW signal sidebands frequencies are much lower than the free spectral range of the arm cavities, i.e. $\Omega L/c \ll 1$. The phase shift introduced by the sloshing cavity, α_{SC}, is defined by the same expression as β_{MI} with γ_{arm} substituted with the half-bandwidth, γ_{SC}, of the sloshing cavity. Thus, one can finally write the following general formula for the optomechanical coupling factor in a sloshing speedmeter as:

$$\mathcal{K}_{SSM}(\Omega) \simeq \frac{4\Theta\gamma_{arm}}{(\Omega^2 - \Omega_s^2)^2 + \gamma_{arm}^2\Omega^2}. \tag{10}$$

where Θ is the normalised intra cavity power for the general sloshing speedmeter.

Assuming a homodyne readout of an arbitrary outgoing light quadrature $\hat{b}_\zeta^{out} = \hat{b}_c^{out} \cos \zeta + \hat{b}_s^{out} \sin \zeta$ and assuming a vacuum state for the incoming field $\hat{a}^{in}$, one can get the following expression (cf equation (20) in [25]) for the power spectral density of quantum noise in the lossless tuned interferometer, characterised by optomechanical coupling factor $\mathcal{K}$ using I/O-relations (4):

$$S^h(\Omega) = \frac{h_{SQL}^2}{2\mathcal{K}(\Omega)} \left[(\mathcal{K}(\Omega) - \cot \zeta)^2 + 1\right] \tag{11}$$

where ζ is the homodyne phase. If one assumes a squeezed vacuum injection instead, the above formula transforms into the following one:

$$S_{sqz}^h = \frac{h_{SQL}^2}{2\mathcal{K}} \left\{e^{2r}(\sin \lambda - \cos \lambda [\mathcal{K} - \cot \zeta])^2 + e^{-2r}(\cos \lambda + \sin \lambda [\mathcal{K} - \cot \zeta])^2\right\}. \tag{12}$$

where r is the squeezing factor and λ is the squeezing angle. In the case of phase squeezing, when $\lambda = 0$, the above formula transforms into a much simpler and intuitive one:

$$S_{sqz}^h = \frac{h_{SQL}^2}{2\mathcal{K}} \left\{e^{2r}(\mathcal{K} - \cot \zeta)^2 + e^{-2r}\right\}. \tag{13}$$

In equation (11), one can see that the term $\propto (\mathcal{K}(\Omega) - \cot \zeta)$, originating from the back action, can be made zero, if $\zeta = \text{arccot}\,\mathcal{K}$. This is the idea behind the well-known variational readout concept that allows us to eliminate the radiation-pressure noise from the readout of the GW interferometer, but the back-action is eliminated only in the absence of loss. However, since $\mathcal{K}(\Omega)$ has a strong dependence on the GW frequency, owing mainly to the mechanical response of the test masses to the radiation pressure force, it is impossible without additional dispersive elements (filter cavities) to achieve the necessary frequency dependence of $\zeta(\Omega)$.

If one is interested in optimising the performance of the GW interferometer predominantly at low frequencies, the speedmeter approach is worthwhile of consideration, since for frequencies below the cavity pole $\Omega < \gamma_{\text{arm}} < \Omega_{\text{s}}$, the optomechanical coupling becomes frequency independent, $\mathcal{K}_{\text{SSM}} \to 4\Theta\gamma_{\text{arm}}/\Omega_{\text{s}}^4 = \text{const}$. In this case the optimal readout quadrature can be obtained, $\zeta_{\text{SSM}}^{\text{opt}} = \text{arccot}\left(4\Theta\gamma_{\text{arm}}/\Omega_{\text{s}}^4\right)$ resulting in a back-action-free sensitivity curve parallel to the SQL line, characteristic of speedmeter behaviour. Phase squeezing is optimal in this case, with $\lambda = 0$, which provides e^{-2r} reduction of noise in the entire back-action-free range of frequencies. It has to be noted though that to overcome the SQL a sufficient amount of optical power has to circulate in the arms exceeding some threshold value, $P_{\text{SSM}}^{\text{crit}}$, defined from the condition $\mathcal{K}_{\text{SSM}}^{\text{crit}} = 1$ that yields

$$P_{\text{SSM}}^{\text{crit}} = \frac{Mc^4 T_{\text{s}}^2}{64\omega_{\text{p}}L_{\text{s}}^2 T_{\text{ITM}}}. \tag{14}$$

The idealised picture above breaks down when one takes different loss into account. Loss in different parts of the interferometer influence different frequency bands, however the effect it has is universal—extra noise is added to the ideal quantum noise budget of a lossless interferometer. This is the direct consequence of the fluctuation-dissipation theorem (FDT) of Callen and Welton [27] that uniquely links any dissipation in the system to a respective source of uncorrelated vacuum fluctuations injected into the system at the lossy element. Since speedmeters, as any quantum noise mitigating devices, rely on quantum correlations of the intracavity light field, any vacuum field mixing in with the intricate intracavity light quantum state ruins those correlations.

We analyse numerically the influence of various sources of loss on the sensitivity of considered schemes hereinafter, yet three main loss mechanisms are common for any scheme and have the largest overall effect on the final sensitivity. These are (i) readout loss, (ii) intracavity loss and (iii) injection loss.

The first one arises due to non-unity quantum efficiency, $\eta - d < 1$, of the photodiodes and boils down to additional vacuum noise added to the readout of the ideal interferometer in the proportion of $\xi_d = \sqrt{1 - 1/\eta_d}$:

$$\hat{b}_\zeta^{\text{out}} = \sqrt{\eta_d}\left(\hat{b}_{\text{c}}^{\text{out}} \cos \zeta + \hat{b}_{\text{s}}^{\text{out}} \sin \zeta\right) + \sqrt{1 - \eta_d}\hat{n}_{\text{vac}}.$$

Intracavity loss manifests as the fractional loss of photons inside the interferometer, covering loss in the arms, mode mismatch between the arms and the sloshing cavities, loss on the beam splitter and such. It can be phenomenologically characterised by the effective photon loss coefficient $\xi_{\text{int}} = \sqrt{A_{\text{loss}}/(1 - A_{\text{loss}})}$ per photon injected. As our numerical study shows (see tables 3 and 4), the greatest impact on performance is observed when loss is introduced between the arms and the sloshing cavity. The reason is clear: the sloshing speedmeter cancels back-action that light inflicts before leaving for the sloshing cavity by re-injecting the very same photons after being reflected with the π-phase shift off the sloshing cavity, thereby applying the same back-action force but with an opposite sign and a time delay defined by Ω_{s}. If a fraction of photons is lost in this transfer and hence substituted by incoherent vacuum fluctuations,

the corresponding fraction of back-action force remains uncompensated, which manifests in additional Michelson-like back-action force scaled by coefficient ξ_{int}, which shows up at low frequencies (cf last term in brackets in (16) below).

Finally, the injection loss influences the performance of the interferometer with squeezed vacuum input. This type of loss encompasses many different mechanisms, including absorption in the injection optics, mode mismatch with the main interferometer, injection optical path instability etc. Despite complex composition, it boils down to the same type of representation as readout loss, namely

$$\hat{a}_{\text{loss}}^{\text{in}} = \sqrt{\eta_{\text{inj}}}\hat{a}^{\text{in}} + \sqrt{1 - \eta_{\text{inj}}}\hat{n}_{\text{vac}},$$

that leads to effectively decreased (increased) (anti-)squeezing factors for light entering the interferometer:

$$e^{-2s_-} = \eta_{\text{inj}}e^{-2r} + (1 - \eta_{\text{inj}}), \; \left(e^{2s_+} = \eta_{\text{inj}}e^{2r} + (1 - \eta_{\text{inj}})\right), \tag{15}$$

where $s_{-(+)}$ is a new (anti-)squeezing factor.

For small enough intracavity loss $\xi_{\text{int}} \ll 1$, one can write down the modified expression:

$$S_{\text{SSM}}^{h,\,\text{loss}} = S_{\text{sqz}}^{h*} + \frac{h_{\text{SQL}}^2}{2} \left\{ \frac{\xi_d^2}{\mathcal{K}_{\text{SSM}} \sin^2 \zeta} + \xi_{\text{int}}^2 \mathcal{K}_{\text{MI}} \right\}, \tag{16}$$

where S_{sqz}^{h*} is the modified expression (12) with (anti-)squeezing coefficient defined by (15):

$$S_{\text{sqz}}^{h*} = \frac{h_{\text{SQL}}^2}{2\mathcal{K}} \left\{ e^{2s_+}(\sin \lambda - \cos \lambda\, [\mathcal{K} - \cot \zeta])^2 + e^{-2s_-}(\cos \lambda + \sin \lambda\, [\mathcal{K} - \cot \zeta])^2 \right\}. \tag{17}$$

Finally, one can show from this expression that in the presence of loss, the optimal values of homodyne readout angle and the squeezing angle change and thus obtain (cf equations (409) and (411) of [28]):

$$\zeta^* = \text{arccot}\left[\frac{\mathcal{K}_{\text{SSM}}}{1 + \xi_d^2 e^{2s_-}}\right] \quad \text{and} \quad \lambda^* = \arctan\left[\frac{\xi_d^2 \mathcal{K}_{\text{SSM}}}{e^{-2s_-} + \xi_d^2}\right] \tag{18}$$

which after insertion in (16) gives:

$$S_{\text{SSM}}^{h,\,\text{opt. loss}} = \frac{h_{\text{SQL}}^2}{2} \left\{ \frac{\xi_d^2 + e^{-2s_-}}{\mathcal{K}_{\text{SSM}}} + \frac{\xi_d^2 \mathcal{K}_{\text{SSM}}}{1 + \xi_d^2 e^{2s_-}} + \xi_{\text{int}}^2 \mathcal{K}_{\text{MI}} \right\}. \tag{19}$$

The above expression is, of course, valid only if both the homodyne angle and the squeezing angle have the optimal frequency dependence (18), which requires additional filter cavities that are beyond the scope of our study. However, since speedmeter's $\mathcal{K}_{\text{SSM}} \to \text{const}$ at low frequencies, this formula represents the behaviour of quantum noise at frequencies below the cavity pole. As our study demonstrates, loss in various elements of the interferometer have different impact.

3. Comparison of lossless sloshing speedmeters

Each of the four configurations shown in figures 1 and 2 was setup in a numerical model based on a set of parameters compatible with the proposed Einstein telescope [5]. In
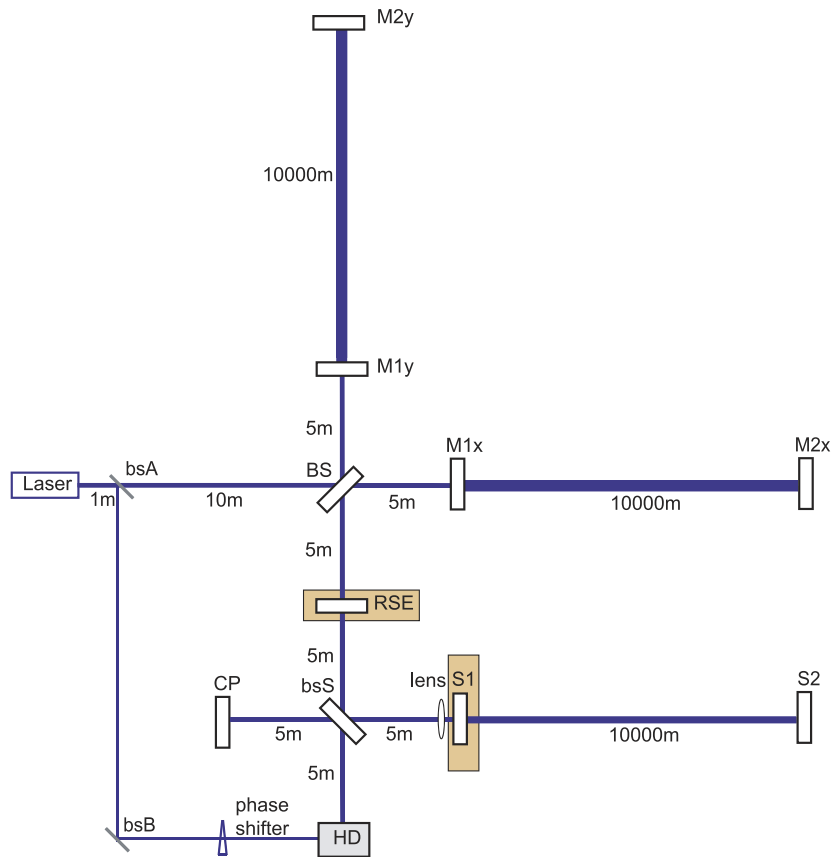
Figure 1. Michelson sloshing speedmeter according to Purdue and Chen. The highlighted mirrors are omitted by Miao (RSE) and Freise (RSE, S1). This schematic includes homodyne detection (HD), and a phase-shifter to set the required local oscillator phase. The lens, which is required to mode-match the system within the Gaussian-beam representation, would most likely be incorporated into the substrate of the input coupler (S1) of the sloshing cavity in a practical implementation. All mirrors have curved surfaces, only the beam-splitters (BS and bsS) are flat. This produces a well mode-matched system.

particular, it was chosen to represent 3 MW of circulating light power in 10 km-long arm cavities, and with the beam-waist of the cavity mode constrained to be in the middle of each cavity. Other parameters of the system were adjusted according to the design principles of the various speedmeter systems. Within these models we consider the effect of three types of loss: mirror loss, beam-splitter loss and cavity-coupling (mode-matching) imperfection. The presence of such imperfections is an important design consideration as without them it would be possible to choose a wide range of parameters that become impractical in their presence.

The simulations presented were conducted in FINESSE [26], a software that has been extensively compared with theory in cases that have convenient analytical solutions. This considerably reduces the burden of accounting for multiple lossy elements within the models, in particular as it allows the effects of imperfect mode-matching to be calculated. To this end,
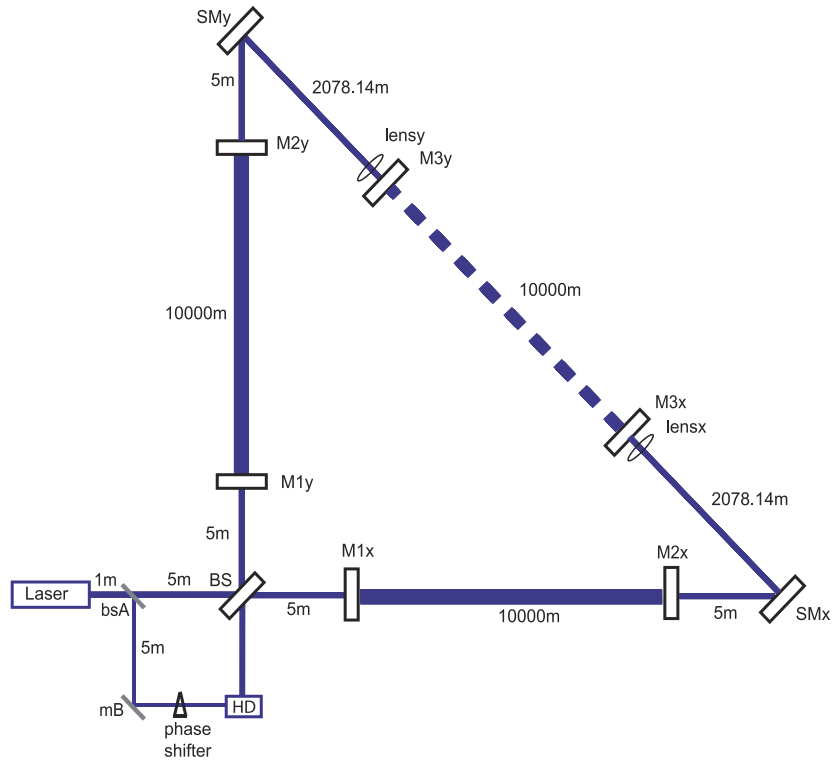
Figure 2. Schematic of the sloshing-Sagnac interferometer. For convenience in modelling, we choose to form the interferometer with the geometry of a right-angle isosceles triangle, without losing applicability to ET. The core interferometer is formed by BS and the two arm cavities formed from four mirrors of the same reflectance (M1x, M2x, M1y, M2y). The end test masses of these resonant arm cavities are linked via steering mirrors (SMx, SMy) to a 10 km long anti-resonant cavity (M3x, M3y). The lenses (lensy, lensx) are required to match the cavity modes and these would most likely be incorporated into the substrates of the adjacent mirrors in a practical implementation. All cavity mirrors have curved surfaces, the beam-splitters and steering mirrors are flat, which produces a well mode-matched system. The signal is read out via the homodyne detector (HD).

we model Gaussian beams and appropriately-curved mirror surfaces to produce an initially well mode-matched system. Loss is introduced by adjusting the curvature of the matching optics to produce the required mismatch. To simulate the opto-mechanical interactions, in which the mirrors are free to move in response to radiation pressure, we represent mirrors suspended as pendulums with a resonant frequency well below the observing band (only a single degree of freedom is represented—that for longitudinal motion in the direction normal to the mirror surface). In the ideal, well mode-matched Michelson sloshing speedmeter, there is no detectable light power (2×10^{-24}W) stored in the sloshing cavity. This is not a problem for the numerical simulations, but was considered to poorly represent a practical arrangement. Therefore, we have chosen to build in one imperfection; a beam-splitter offset of $0.0001°$. This brings the light power in the Michelson sloshing speedmeters up to the micro-watt level, but does not influence the sensitivity significantly. We apply the same imperfection to the sloshing Sagnac,
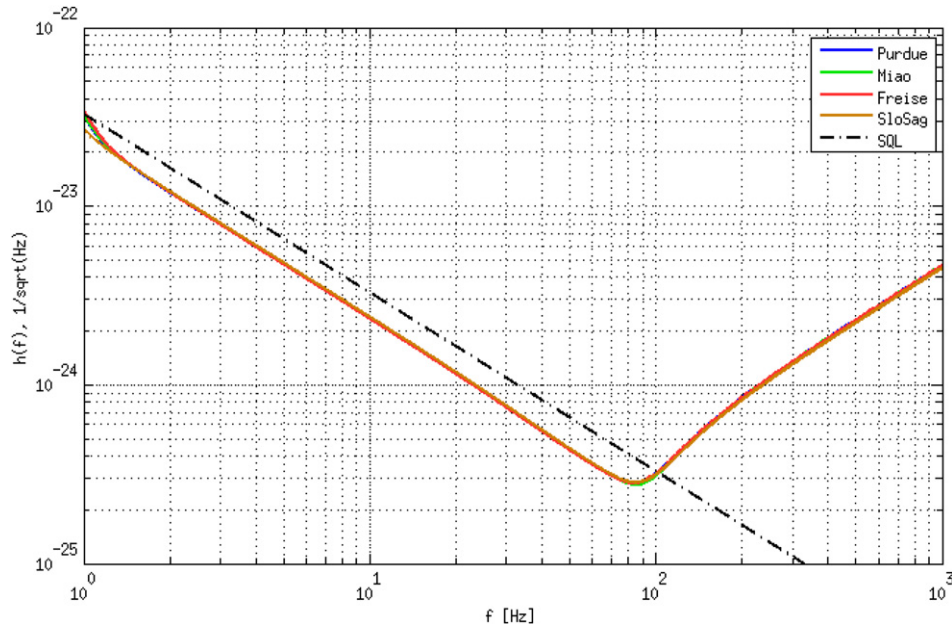
Figure 3. Sensitivity curves for our sloshing speedmeters. Here it can be seen, that the curves lie almost on top of each other, except the curve of the sloshing Sagnac leaves the common trend from 0 to 0.4 Hz. All these curves were optimised for a detection frequency of 10 Hz.

to ensure a fair comparison. In the following sections, we describe the process of modelling each system in turn.

3.1. Michelson sloshing speedmeter

A schematic of Purdue and Chen's interferometer is given in figure 1. The mirrors omitted by Miao and Freise to achieve the simplified configurations are highlighted.

Initially, we model ideal, lossless mirrors. The reflectance of the end test masses (M2x, M2y and S2) and the closed port (CP) are unity. The main beam-splitter (BS) has a transmittance of 0.5. For all other mirrors the transmittance must be optimised to achieve the desired frequency response and speedmeter behaviour. These mirrors are the input couplers of the arm cavities (M1x, M1y), the resonant side band extraction mirror (RSE), the extraction mirror (bsS) and the input coupler of the sloshing cavity (S1).

In the Purdue and Chen arrangement, the input couplers of the arm cavities and the RSE mirror are specified to have the same transmittance. When this constraint is applied, in the lossless case, the shape of the sensitivity curve is entirely determined by the choice of the transmission of S1 and bsS. For Miao's speedmeter, omitting the RSE mirror leaves only the input couplers of the arm cavities, the extraction mirror and the input coupler of the sloshing cavity to adjust. Finally, omitting the RSE and the S1 mirror as done by Freise, we have only the transmittance of the arm cavity input couplers and the extraction mirror to choose.

As there is an indefinite number of different solutions to achieve a speedmeter response, where the sensitivity curve follows the standard quantum limit, it was necessary to introduce an additional constraint: the sensitivity curves should follow the standard quantum limit

Table 1. Parameters for the different Michelson speedmeters in the initial simulations with lossless mirrors and beam-splitters. The sensitivity curve for the speedmeter according to Purdue and Chen is independent of the transmittance of the mirrors M1 and RSE as long they have the same value. This is not the case for Miao's and Freise's speedmeter, where the RSE mirror is omitted. In the following sections we change only the loss of the individual optical components. Since the sum of the transmittance, reflectance and loss is unity, the reflectance of the individual component gets reduced by the specified loss.

	Purdue & Chen	Miao	Freise
Transmittance (—)			
M1	0.07	0.07	0.07
RSE	0.07	—	—
bsS	0.0178	0.9485	0.9828
S1	0.0013	0.75	—
BS	0.5	0.5	0.5
M2	0	0	0
S2	0	0	0
CP	0	0	0
Losses (—)			
All components	0	0	0
Focal length (m)			
Lens	2782.15	2782.15	2782.15
Light power (W)			
In the arm cavities	3×10^6	3×10^6	3×10^6
In the sloshing cavities	9.7×10^{-6}	9.7×10^{-6}	9.7×10^{-6}
Offset (deg)			
BS	0.0001	0.0001	0.0001
Laser wavelength (nm)			
Nd:YAG	1064	1064	1064

up to 80 Hz, and overlap at higher frequencies. We proceeded by fixing the transmittances of the input couplers of all the interferometers to 0.07, and the same value was chosen for the RSE mirror for Purdue and Chen's speedmeter. The value chosen is unimportant for the lossless case of the Purdue and Chen configuration, since the interferometer is impedance-matched, and therefore independent of the actual transmission of the input couplers and the RSE mirror. However, the particular choice becomes significant when loss is present, and hence was made in anticipation of the effect of loss. In addition, with the chosen value, all the speedmeters then operate with the same laser input power. Working from that basis, we then found the remaining transmittances for all the other mirrors, and for each design, so that their sensitivity curves overlap as shown on figure 3. The resulting parameters are listed in the table 1.

In the process of simulating the various options, we next optimise the local oscillator phase to maximise the sensitivity. As noted above, we have chosen to carry out this optimisation at a target frequency of 10 Hz. The choice of optimisation frequency has only a marginal effect on the outcome compared to other frequencies well below the chosen upper limit of 80 Hz. The closely-matched sensitivity curves obtained in the lossless case form a basis for the further exploration of the models including loss and squeezing. We note that the optimisation carried

Table 2. Parameters of the sloshing Sagnac interferometer using lossless mirrors/beam-splitters. In the following sections we change only the loss of the individual optical components. Since the sum of the transmittance, reflectance and loss is unity, the reflectance of the individual component gets reduced by the specified loss.

Transmittance (—)	
BS	0.5
SMx/y	0
M1x/y, M2x/y	0.07
M3x/y	0.035
Loss (—)	
All components	0
Focal length (m)	
Lensx/y	3043.33
Light power (W)	
In the resonant arm cavities	3×10^6
In the anti-resonant cavity	485
Offset (deg)	
BS	0.0001
Laser wavelength (nm)	
Nd:YAG	1064

out in this work was done by searching on a fine grid within the relevant parameter space and maximising the snr at 10 Hz.

3.2. Sloshing Sagnac speedmeter

In a previous paper [16], we have dealt extensively with the ideal, lossless sloshing Sagnac speedmeter, and we refer to this paper for the detail. Here we present the schematic layout (figure 2), and the modified optical parameters (table 2) required to achieve the same performance as the Michelson sloshing speedmeters, see figure 3. The approach to optimisation and fitting is the same as those for the sloshing Michelson case.

4. The effect of optical loss on four speedmeter designs

In this section, we discuss the effect of incorporating loss into our model of the four speedmeters under consideration. The individual loss values chosen for mirrors and beam-splitters are considered to be a realistic estimate of values that should be typically available in the construction of the next generation of gravitational wave detectors (i.e. lower than currently available by a small factor).

Starting with the Michelson sloshing speedmeters, we have chosen a loss of 30 ppm for all mirrors (M1, M2, RSE, S1, S2, CP), a loss of 100 ppm for all beam-splitters (BS, bsS), a 99 % detection efficiency and a loss of 1 % due to mode matching error. The mode matching error is inserted by changing the focal length of the lens by 1 %. For the sloshing Sagnac speedmeter, the same loss values apply. Since we have two lenses in the sloshing Sagnac we have chosen to insert the mode mismatch at one lens only, as for the Michelson speedmeters.
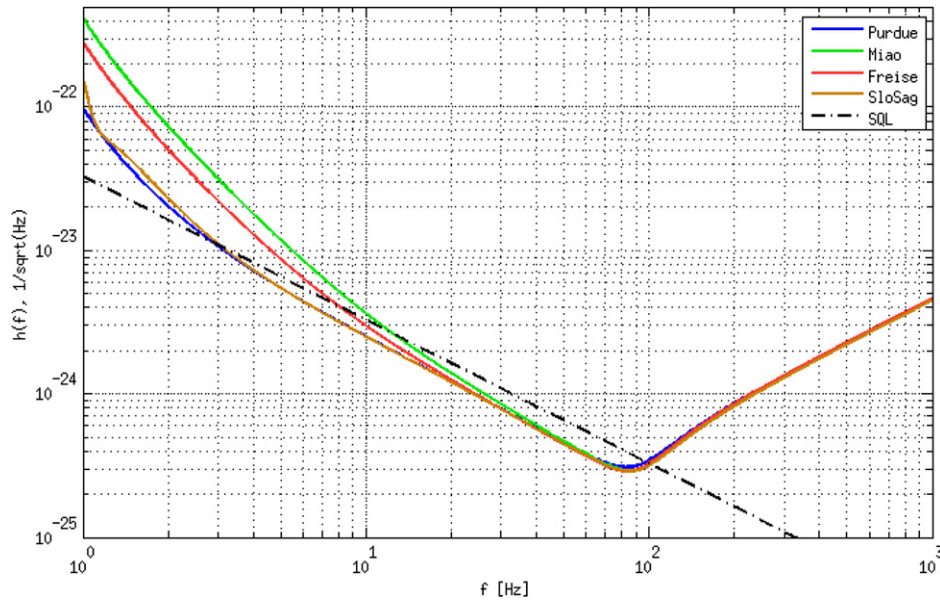
Figure 4. Sensitivity curves for the different sloshing speedmeters with all the individual loss, as specified in tables 3 and 4, inserted. The curves are optimised for the local oscillator phase at a detection frequency of 10 Hz.

Generally it can be said that with the introduction of loss in any interferometer, the stored light power is reduced. Usually, in a practical implementation, the maximum light power is limited by thermal distortion and not by the available power, therefore we choose to re-adjust the injected light power to keep the circulating light power at 3 MW, for a fair comparison. Then, by inserting all the loss into our simulations, we obtain the sensitivity curves shown in figure 4. It should be noted, that the mirror parameters were not re-adjusted after the loss values were inserted.

With the chosen values of loss, the situation changes: the sensitivity curves for the different designs show differences in particular in the frequency range between 1 Hz and 20 Hz, corresponding to the re-introduction of back-action noise into the QND measurement. As described above, these curves were optimised for a detection frequency of 10 Hz. The choice of this frequency, within the band described above, does not materially affect the result in the case of a system with loss. When one compares the magnitude of the sensitivity curves at a high frequency, e.g. 1000 Hz, one can see that there the curves are not affected by the optimisation 10 Hz. It can be seen that there is almost no difference in performance in the presence of loss between the sloshing Sagnac speedmeter and the speedmeter from Purdue and Chen. The speedmeters from Freise and Miao exhibit increased degradation of performance in the presence of loss.

By inserting only one individual loss source at a time and comparing the result with our previous lossless simulations, we found the sensitivity degradation due to each separate optical component and identified that with the biggest influence on the loss budget. The loss factor is determined by equating the ideal (lossless) sensitivity to 100 % and, using the rule of three[5] to

---

[5] $x\% =$ loss value/lossless value $\times$ 100%—the loss value and the lossless value are from the simulation.

Table 3. Michelson sloshing speedmeters: difference in percentage[6] from the ideal sensitivity curve when inserting only one individual loss. For completeness we have inserted the total loss (all losses) in the table. For each of these values, the sensitivity curve was optimised for 10 Hz, homodyne phase was adjusted, and the arm-cavity power was maintained at 3 MW.

Optics	Loss	Purdue & Chen	Miao	Freise
BS	100 ppm	0.17	0.16	0.17
M1x/y (common)	30 ppm	0.05	0.05	0.05
M1x/y (differential)	60 ppm/0 ppm	0.05	0.05	0.05
M2x/y (common)	30 ppm	0.02	0.02	0.02
M2x/y (differential)	60 ppm/0 ppm	0.02	0.02	0.02
RSE	30 ppm	0.05	—	—
bsS	100 ppm	0.14	2.97	8.96
CP	30 ppm	0	0.46	1.46
S1	30 ppm	1.49	1.90	—
S2	30 ppm	1.46	1.43	1.48
Detection	1%	0.98	0.95	0.99
Mode matching (via lens)	1%	2.67	47.57	16.50
All losses		6.84	52.49	27.33

Table 4. Sloshing Sagnac speedmeter: difference in percentage[6] from the ideal sensitivity curve when inserting only one individual loss. For completeness we have inserted the total loss (all losses) in the table. For each of these values, the sensitivity curves are optimised for 10 Hz and the arm cavities power was kept at 3 MW.

Optics	Loss	Sloshing Sagnac
BS	100 ppm	0.01
M1x/y (common)	30 ppm	0.02
M1x/y (differential)	60 ppm/0 ppm	0.02
M2x/y (common)	30 ppm	0.05
M2x/y (differential)	60 ppm/0 ppm	0.05
M3x/y	30 ppm	2.72
SMx/y	30 ppm	0.05
Detection	1%	0.94
Mode matching (via lens)	1%	0.49
All losses		3.62

calculate the relative sensitivity for the lossy system in terms of a percentage. The outcomes[6] are given in tables 3 and 4. The sum of the individual loss factors gives approximately the total loss factor. The small discrepancy is due to the complex interactions within the coupled-cavity systems that lead to slightly different levels of optical power other than in the arm cavities where the power is kept constant at 3 MW.

For all the Michelson sloshing speedmeters the dominant loss source is due to the mode-matching error. In the sloshing Sagnac the biggest individual loss factors come from the mirrors M3x and M3y. The presence of coupled cavities also explains that, when we add loss on ITMx

---

[6] Difference in % = $x\% - 100\%$.
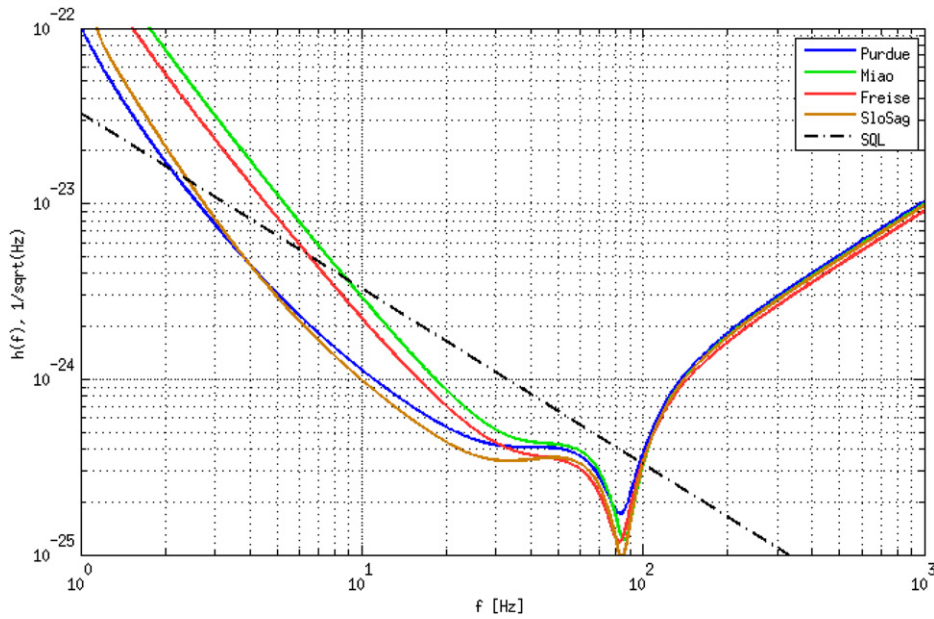
Figure 5. Sensitivity curves for lossy speedmeters when applying a 10 dB squeezing. The curves are simultaneously optimised for the local oscillator phase and the squeezing angle at a detection frequency of 10 Hz.

or ITMy, this has a greater effect that when we apply the same loss to ETMx or ETMy (in the latter case only the power within the arm cavity is affected, and this is held constant as explained above).

5. The effect of squeezing on four speedmeter designs

In this section, we present the response of the four lossy speedmeters to squeezing. Generally, appropriately-adjusted squeezing in speedmeters pushes the low-frequency (speedmeter-response) part of the sensitivity curve down, at the cost of a deterioration at the high-frequency part at and above the arm-cavity corner frequency, where the squeezing phase chosen for low-frequency is not optimal. We include in our models the loss specified in tables 3 and 4. In addition we apply 10 dB of squeezing in the model of the read-out system of the detector.

To accomplish this in the Michelson speedmeters, squeezed light is injected (in the model) between the extraction mirror (bsS) and the homodyne detector (HD) via a model-element representing a Faraday isolator. For the sloshing Sagnac speedmeter, the corresponding point of injection is between the beam-splitter (BS) and the homodyne detector (HD). To obtain the best sensitivity for each speedmeter type, we optimise the local oscillator phase and the squeezing angle at a frequency of 10 Hz, as given in figure 5, and following the principles described in the earlier sections.

Loss limits the gain in sensitivity that can be obtained through the application of squeezing in a frequency-dependent manner. In the region below approximately 20 Hz, with the assumed levels of loss, none of the speedmeters reaches the full potential from squeezing (i.e. 10 dB improvement). The sensitivity curves, while still optimised at 10 Hz, show an overall

improvement at frequencies up to approximately 100 Hz, we re-iterate that these curves represent frequency-independent squeezing. The decrease in improvement at higher frequencies could be avoided by applying frequency-dependent squeezing, considered to be beyond the scope of the present work. The main observation arising from these results is that the performance in the presence of loss and squeezing improves in line with increasing complexity of the speedmeter.

6. Conclusion

The starting point for the current exploration was to establish equivalent speedmeters of each class, with almost identical sensitivity curves. By equivalent speedmeters we mean we used the same arm cavity length and the same circulating light power in the arm cavities. We have chosen to make the transmissions of the input couplers the same, which corresponds that all our investigated speedmeters have the same input power at the laser. Then we found the values of the remaining mirrors. The remaining mirrors vary in number from one to three, such that the more mirrors a speedmeter type has, the more design-freedom there is. However, this freedom comes at the cost of more complexity in construction and in the control system required to keep the cavities on resonance or anti-resonance, and therefore it is important to consider whether the extra complexity of one type over another is merited, or under which circumstances it may be.

The outcome of this comparison of four speedmeter configurations indicates that their sensitivity to gravitational waves is identical for the chosen parameters when no loss is considered. With lossy optics, however, the situation changes: now the sloshing Sagnac and the speedmeter of Purdue and Chen display the best (essentially identical) sensitivities when optimised at 10 Hz, followed in performance terms by Freise's and Miao's speedmeters. With the insertion of 10 dB squeezing in our lossy speedmeters, the sensitivity improves; but the improvement is greater for the more complex speedmeters. In this situation, the sloshing Sagnac displays the best performance, followed by the speedmeter from Purdue and Chen.

With regard to the optimisation frequency of 10 Hz, by sampling cases for each speedmeter type, optimised for lower or higher frequency, we obtained results that differed only slightly for reasonable changes in optimisation frequency within the band in which the systems operate as speedmeters. We carried out our analysis in the context of the proposed Einstein telescope, for only one set of parameters. Had we chosen a different set of parameters, such as by lifting the constraint placed on Purdue and Chen's speedmeter that the input couplers of the arm cavities and the extraction mirrors should have the same transmission, or made other changes of this kind, the outcomes may be different. This work is, therefore, best considered to be an initial evaluation of the performance of a potentially interesting subset of speedmeters: the sloshing speedmeters.

ORCID iDs

S H Huttner ⓘ https://orcid.org/0000-0002-6575-4888

References

[1] Abbott B P *et al* 2016 *Phys. Rev. Lett.* **116** 061102
[2] Acernese F *et al* 2015 *Class. Quantum Grav.* **32** 024001
[3] Aso Y *et al* 2013 *Phys. Rev. D* **88** 043007
[4] LIGO-India 2011 Proposal of the Consortium for Indian Initiative in Gravitational-wave Observations (IndIGO), 2011, LIGO Document M1100296-v2 https://dcc.ligo.org/M1100296/public
[5] Punturo M *et al* 2010 *Class. Quantum Grav.* **27** 194002
[6] Abbott B P *et al* 2017 *Class. Quantum Grav.* **34** 044001
[7] Braginsky V B and Khalili F J 1990 *Phys. Lett.* A **147** 251
[8] Braginsky V B *et al* 2000 *Phys. Rev.* D **61** 044002
[9] Purdue P 2002 *Phys. Rev. D* **66** 022001
[10] Purdue P and Chen Y 2002 *Phys. Rev. D* **66** 122004
[11] Chen Y 2003 *Phys. Rev. D* **67** 122004
[12] Danilishin S L 2004 *Phys. Rev. D* **69** 102003
[13] Danilishin S L 2010 GWADW-2010 Kyoto
[14] Wade A R *et al* 2012 *Phys. Rev. D* **86** 062001
[15] Wang M *et al* 2013 *Phys. Rev. D* **87** 096008
[16] Huttner S H *et al* 2017 *Class. Quantum Grav.* **34** 024001
[17] Danilishin S L *et al* 2018 *Light: Sci. Appl.* **7** 11
[18] Miao H 2010 *PhD Thesis* University of Western Australia
[19] Freise A 2016 *Presentation at the Speedmeter Workshop* (Scotland: Edzell)
        Freise A, Miao H and Brown D D 2020 *Class. Quantum Grav.* **37** 025007
[20] McKenzie M *et al* 2002 *Phys. Rev. Lett.* **88** 231102
[21] Caves C M 1981 *Phys. Rev. D* **23** 1693
[22] Kimble H J *et al* 2002 *Phys. Rev. D* **65** 022002
[23] Caves C M and Schumaker B L 1985 *Phys. Rev.* A **31** 3068
[24] Schumaker B L and Caves C M 1985 *Phys. Rev.* A **31** 3093
[25] Danilishin S L, Khalili F Y and Miao H 2019 *Living Rev. Relativ.* **22** 2
[26] Brown D D and Freise A 2014 Finesse, Frequency domain interferometer simulation software (http:gwoptics.org/finesse)
[27] Callen H and Welton T 1951 *Phys. Rev.* **83** 3440
[28] Danilishin S L and Khalili F Y 2012 *Living Rev. Relativ.* **15** 5